Jurnal Teknik Industri, Vol. 28, No. 2, December 2026 DOI: https://doi.org/10.9744/jti.28.2.117-138
ISSN 1411-2485 print / ISSN 2087-7439 online

Hybrid Surrogate - Physics - AI Optimization of EPB-TBM Performance: A Data-Driven Application

Maharani Rindu Widara[1]*, Chairul Salam M[2]
[1)] Mining Engineering, Politeknik Batulicin, South Kalimantan, 72271, Indonesia
[2)] Istanbul Technical University, Maslak, Istanbul, 34469, Turkey
Email: maharani@politeknikbatulicin.ac.id*
*Corresponding author

Abstract: The increasing complexity and geological unpredictability associated with mechanized tunneling demand optimization frameworks that go beyond static, offline parameter adjustments and embrace adaptive and physically coherent decision-making processes. Traditional metaheuristic algorithms, such as genetic algorithms (GA), particle swarm optimization (PSO), and simulated annealing (SA), have been widely applied to optimize tunnel boring machine (TBM) performance. However, they are inherently limited by their lack of real-time adaptability and restricted physical interpretability. This research presents a hybrid surrogate–physics–AI optimization framework (H-SGP-BO–PINN–DRL) that redefines TBM optimization as a physics-constrained adaptive control challenge, shifting away from a static optimization model. The framework integrates a surrogate-assisted hybrid GA–PSO combined with Bayesian optimization for a global search that considers uncertainty, a physics-informed neural network (PINN) that incorporates essential mechanical principles to ensure geotechnical feasibility, and a deep reinforcement learning (DRL) controller that enables cycle-wise adaptive adjustments within physically feasible operational limits. The framework was validated using field data from EPB-TBM projects in the Jakarta MRT and Istanbul Metro systems, as well as synthetic datasets generated using FEM. The results show that the proposed method reduces the specific energy consumption (SEC) and improves the penetration rate (PR), while also demonstrating superior convergence stability and robustness compared to traditional metaheuristic and surrogate-based methods. Monte Carlo bootstrapping and Sobol global sensitivity analysis further identify thrust force and cutterhead rotation speed as the main factors affecting energy-performance variability. By integrating surrogate-assisted optimization, physics-informed learning, and reinforcement-based adaptability, this study introduces a new paradigm for intelligent TBM operation, enabling interpretable, energy-efficient, and deployable decision support for future smart and autonomous tunneling systems.

Keywords: Tunnel Boring Machine (TBM) optimization, hybrid surrogate - physics - AI framework, physics-informed neural network (PINN), deep reinforcement learning (DRL), Bayesian evolutionary optimization.

Introduction

Tunnel boring machines (TBMs) are central to modern underground infrastructure development, where operational efficiency directly governs the project duration, energy consumption, and excavation cost. As tunneling projects increasingly encounter heterogeneous and uncertain ground conditions, the limitations of traditional rule-based and experience-driven operations have become more pronounced. Data-driven optimization techniques have been extensively adopted to improve TBM performance, particularly with respect to minimizing the specific energy consumption (SEC) and maximizing the penetration rate (PR) [1], [2], [3]. Over the past decade, metaheuristic algorithms, including genetic algorithms (GAs), particle swarm optimization (PSO), and simulated annealing (SA), have been effective in identifying improved combinations of operational parameters. However, these methods are inherently static and offline and rely on fixed objective functions and predefined search spaces. Consequently, they exhibit limited adaptability to evolving geological conditions, weak physical interpretability, and declining robustness in high-dimensional or uncertain environments [4], [5], [6], [7]. Given these methodological constraints, the evolution of TBM optimization research has shifted toward frameworks that integrate artificial intelligence, surrogate modeling, and physics-based constraints to achieve adaptive and physically consistent performance improvements in the tunneling process.

Submitted: April 11, 2026; Revised: July 05, 2026; Accepted: Aug 07, 2026

Over the past decade, numerous studies have employed metaheuristic algorithms, such as genetic algorithms (GA), particle swarm optimization (PSO), and simulated annealing (SA), to enhance the performance of tunnel boring machines (TBMs). These approaches have been applied to improve the parameters related to energy consumption, penetration rate, and operational stability under varying geological conditions. Despite their success, most previous studies have been characterized by static optimization and limited adaptability to dynamic environments. Moreover, the integration of physical constraints and uncertainty quantification is insufficient. Previous studies have demonstrated that various metaheuristic algorithms, including GA, PSO, and SA, have been extensively applied to optimize TBM performance with varying degrees of success. Although these classical methods effectively improve energy efficiency and penetration rates, their adaptability to dynamic geological conditions remains limited. As research has evolved, hybrid and physics-informed approaches have been developed to overcome these constraints by improving convergence efficiency, physical consistency, and real-time learning capabilities. Here, dynamic geological conditions refer to the spatial heterogeneity encountered progressively along the tunnel alignment, such as transitions between soil layers of differing UCS and moisture content across successive excavation rings, rather than second-by-second temporal change; classical metaheuristics re-optimize offline for a fixed geological assumption and cannot adjust once the encountered ground departs from that assumption [8].

Research Gap

Although numerous studies have focused on optimizing TBM performance using heuristic and metaheuristic techniques, several critical research gaps remain unaddressed. First, most existing approaches are designed for static or offline optimization, in which parameter adjustments are performed post-analysis rather than continuously during the excavation. This static approach limits the real-time adaptability and responsiveness to rapidly changing subsurface conditions [9], [10], [11]. Second, uncertainty and parameter interactions have often been neglected in previous optimization frameworks. The interdependence among mechanical and operational variables, such as thrust, torque, and pressure, introduces nonlinear and probabilistic behaviors that cannot be effectively captured by deterministic optimization alone. Consequently, predictions may exhibit significant deviations under real-world conditions [12], [13], [14]. Third, the integration between physics-based modeling and AI-driven adaptive control in TBM studies is limited. Most algorithms optimize empirical relationships without incorporating the governing physical laws of the ground–machine interaction. The absence of physics-informed learning restricts the reliability and generalizability of optimization outcomes, particularly under geotechnical uncertainty [15], [16], [17]. To overcome these limitations, a more comprehensive and hybridized optimization approach that combines physical understanding, probabilistic reasoning, and adaptive intelligence into a unified framework is required. Accordingly, this study contributes: (i) a surrogate-assisted hybrid GA-PSO-BO global search layer that reduces reliance on expensive FEM evaluations; (ii) a physics-informed constraint layer (PINN) that enforces mechanical equilibrium and boundary conditions on candidate solutions; and (iii) a DRL-based cycle-wise adaptive decision layer, jointly validated using combined field data from the Jakarta MRT and Istanbul Metro projects and FEM-simulated data.

Methods

Metaheuristic Optimization in TBM

Over the past decade, metaheuristic algorithms have been extensively applied to optimize tunnel boring machine (TBM) performance parameters, particularly between 2010 and 2022. Classical optimization techniques, such as genetic algorithms (GA), particle swarm optimization (PSO), and simulated annealing (SA), have been widely utilized to determine the optimal combination of operational variables, including thrust force, cutterhead speed, and face pressure. These methods are primarily employed to minimize the specific energy consumption (SEC) and maximize the penetration rate (PR) through iterative search mechanisms inspired by natural or physical processes [18], [19]. Despite their success in providing feasible operational guidelines, traditional metaheuristics have several inherent limitations. They tend to be computationally expensive when dealing with high-dimensional objective functions and exhibit strong dependency on parameter tuning. Furthermore, owing to their stochastic nature, convergence toward the global optimum is not always guaranteed, and local optimum trapping remains a persistent issue. As TBM systems become more complex and data-rich, the lack of adaptability and predictive learning capabilities in conventional metaheuristic approaches increasingly restricts their applicability [20], [21]. To address these computational and convergence challenges, subsequent studies have explored the integration of surrogate-assisted and Bayesian-based optimization frameworks that enhance efficiency without compromising solution accuracy.

Surrogate-Assisted and Bayesian Optimization

Surrogate-assisted optimization has emerged as a promising alternative for handling expensive function evaluations in complex engineering systems. Techniques such as Gaussian process regression (GPR), kriging, and radial-base function (RBF) modeling have been employed to approximate objective functions based on a limited number of high-fidelity simulations. These surrogate models act as computationally efficient proxies that guide the search process toward the optimal regions of the solution space with a reduced computational burden [22], [23]. Recent studies conducted between 2023 and 2025 have demonstrated that the combination of surrogate modeling and Bayesian optimization (BO) significantly improves convergence efficiency in multi-objective and nonlinear problems. Bayesian methods use probabilistic inference to balance exploration and exploitation through acquisition functions, such as expected improvement (EI) or upper confidence bound (UCB). In tunneling and other large-scale mechanical systems, this approach has been shown to accelerate optimization processes by reducing the number of expensive physical or numerical evaluations required [24], [25]. Building on this foundation, the integration of physical knowledge into data-driven models has been increasingly recognized as essential for ensuring that learned relationships remain consistent with the governing laws of mechanics and material behavior.

Physics-Informed Neural Networks (PINN)

Physics-informed neural networks (PINNs) have recently gained attention owing to their ability to directly integrate governing equations into the learning process. Unlike purely data-driven approaches, PINNs incorporate partial differential equations that represent mechanical equilibrium, stress–strain rela–tionships, and boundary conditions as soft constraints in the loss function. This hybridization enables neural networks to adhere to the physical laws while learning from empirical or simulated data. In the context of TBM operations, the incorporation of governing equations related to the thrust force, cutterhead torque, and face pressure is particularly relevant because TBM continuously interacts with heterogeneous and nonlinear geotechnical media. The use of PINNs ensures that the predicted operational parameters not only minimize energy consumption but also remain mechanically feasible under complex subsurface conditions. Although PINNs provide physical consistency in predictive modeling, adaptive control and decision-making under dynamic geological variability require an additional layer of real-time learning and policy optimization, which has been addressed by recent advancements in deep reinforcement learning [26], [27].

Deep Reinforcement Learning in Tunneling Automation

Recent developments in deep reinforcement learning (DRL) have introduced advanced capabilities for dynamic control and adaptive optimization in tunneling systems. Algorithms such as proximal policy optimization (PPO), soft actor–critic (SAC), and deep deterministic policy gradient (DDPG) have been successfully applied to continuous control tasks, wherein system parameters evolve in response to changing environmental conditions. In tunneling automation, DRL enables the TBM to learn control policies that maximize performance rewards, such as increased penetration or reduced energy usage, based on real-time feedback loops. Several studies have reported that DRL can significantly improve decision-making in complex and uncertain environments. The ability to map high-dimensional state and action spaces allows for the real-time adaptation of thrust, torque, and pressure parameters, effectively transforming traditional static optimization into a closed-loop intelligent control system. The integration of learning-based control offers an opportunity to enhance the responsiveness and robustness of TBM operations under varying ground conditions [28], [29]. These advancements in metaheuristic optimization, surrogate modeling, physics-informed learning, and reinforcement-based control collectively reveal progress toward a new generation of hybrid frameworks that unify efficiency, physical consistency, and adaptability.

Data Sources and Experimental Setup

In this study, datasets comprising field data from mechanized tunneling projects in the Jakarta MRT and synthetic data generated using finite element method (FEM) simulations were employed. The integration of empirical and simulated data enabled a broader representation of geological conditions. The input parameters included the thrust force, cutterhead speed, face pressure, uniaxial compressive strength (UCS), and moisture content, whereas the output variables comprised the specific energy consumption (SEC) and penetration rate (PR). To ensure data comparability, z-score normalization was applied, and outlier detection was performed using the interquartile range criterion. To establish the optimization framework, the relationship between the operational variables and performance indicators was formalized using a multi-objective mathematical model [30], [31].

Table 1. Data summary: Statistical characteristics of combined field and simulation data

Parameter	Unit	Data source	Mean	Standard deviation	Minimum	Maximum
Thrust force	kN	Field + FEM	6,850	1,240.0	4,200.0	9,500.0
Cutterhead rotation speed (RPM)	rpm	Field + FEM	6.5	1.1	4.2	8.3
Face pressure	bar	Field + FEM	2.4	0.6	1.2	3.8
Torque	kN·m	Field + FEM	980	185.0	640.0	1,280.0
Uniaxial compressive strength (UCS)	MPa	Field	52.0	14.5	25.0	78.0
Moisture content	%	Field	18.5	4.3	10.0	25.0
Specific energy consumption (SEC)	kWh/m^3	Field + FEM	921.9	129.8	800.0	1250.0
Penetration rate (PR)	mm/rev	Field + FEM	7.8	1.6	4.5	10.5

The dataset used in this study comprised field measurements from EPB-TBM tunneling projects in Jakarta and Istanbul and synthetic data generated using finite element method (FEM) simulations. Several operational and geotechnical parameters were selected as inputs to represent the mechanical and environmental conditions that influence the TBM performance. The corresponding output parameters were defined to quantify energy efficiency and excavation productivity. Among the input parameters, the thrust force and cutterhead rotation speed were identified as the most influential factors governing the energy consumption and penetration rate, as they directly control the interaction between the cutterhead and ground material. Face pressure and torque serve as stability and resistance indicators, respectively, reflecting the response of the TBM to varying ground conditions. The uniaxial compressive strength (UCS) and moisture content represent the intrinsic geological properties that determine the cutting resistance and deformation characteristics of the surrounding medium. On the output side, the specific energy consumption (SEC) provides a quantitative measure of tunneling energy efficiency, whereas the penetration rate (PR) reflects the mechanical productivity of the excavation process. Together, these outputs establish a dual-objective performance metric that forms the basis of subsequent optimization. The relationship between the inputs and outputs underscores the necessity of adopting hybrid optimization and machine-learning frameworks capable of capturing nonlinear dependencies, ensuring physical consistency, and adapting to varying operational and geological scenarios.

To ensure comprehensive model calibration, a combined dataset consisting of both field measurements and simulation-derived data was analyzed. The inclusion of empirical data from EPB-TBM projects in Jakarta and synthetic data generated using finite element method (FEM) simulations provided a representative range of operational and geological conditions. Statistical indicators, such as the mean, standard deviation, and range, were calculated to evaluate data variability and consistency. A summary of these statistical characteristics is presented in Table 1.

The statistical summary presented in Table 1 illustrates the variability and representativeness of the combined field and simulation datasets used in this study. The integration of field measurements and FEM-generated synthetic data resulted in a balanced distribution of the operational and geological parameters. The thrust force and torque values exhibited moderate standard deviations, indicating controlled variations in the machine operation while capturing realistic fluctuations in the tunneling conditions. The cutterhead rotation speed and face pressure parameters showed relatively narrow ranges, suggesting consistent operational management during the excavation. In contrast, UCS and moisture content displayed higher variability, reflecting the natural heterogeneity in ground conditions along the tunnel alignment. The output parameters, specific energy consumption (SEC) and penetration rate (PR), demonstrated stable mean values with moderate dispersion, signifying reliable measurement consistency between the field and simulated data. These statistical characteristics confirm that the dataset encompasses a realistic operational domain that is suitable for model training and validation. The observed variability also ensures that the proposed hybrid optimization framework can effectively learn from diverse scenarios, thereby enhancing its robustness, adaptability, and predictive accuracy in real-world TBM applications.

Problem Formulation

The optimization problem was formulated as a bi-objective function that simultaneously minimized energy consumption and maximized the penetration rate. This can be expressed mathematically as

$$minF(x)=[f_1(x)=SEC, f_2(x)=\text{-}PR] \tag{1}$$

where represents the energy objective and represents the productivity objective. $f_1(x) f_2(x)$ The optimization is subjected to physical constraints that govern the operational safety of the Tunnel Boring Machine (TBM):

$$g_1(x): T_{max} < T_{limit}, g_2(x): P_{face} \in [P_{min}, P_{max}] \quad (2)$$

where T_{max} is the cutterhead torque measured and P_{face} is the applied face pressure.

To efficiently evaluate this multi-objective problem while reducing the computational cost, a surrogate modeling approach was adopted in the subsequent stage [32], [33].

Surrogate Modeling Layer

A Gaussian Process Regression (GPR) model was constructed to serve as a surrogate for the computationally expensive FEM simulations of SEC and PR. The surrogate model approximated the true objective functions and through probabilistic inference, defined as:

$$\hat{f}(x) = \mu(x) + k(x, X)[K(X, X) + \sigma_n^2 I]^{-1}(y - \mu(X)) \quad (3)$$

The mean prediction is represented by $\mu(x)$, while the covariance kernel is denoted by $k(x, X)$, and the covariance matrix of the training data is indicated by $K(X, X)$ [34]. To efficiently tackle the bi-objective optimization problem while reducing computational expenses, surrogate modeling techniques were employed to approximate the intricate nonlinear relationships between input variables and target responses, specifically the specific energy consumption (SEC) and penetration rate (PR). By utilizing surrogate models, the hybrid optimization framework can substitute computationally intensive finite element method (FEM) simulations with rapid, data-driven estimates, thus speeding up convergence without compromising accuracy. In this study, three surrogate modeling techniques were explored: Gaussian process regression (GPR), ordinary kriging, and radial basis function (RBF) networks. Each model was trained and validated using a combined dataset of field and synthetic data, as described in the previous section. Their predictive capabilities were evaluated using three statistical metrics: R^2, root mean square error (RMSE), and mean absolute error (MAE), which were calculated separately for SEC and PR. All metrics reported in Table 2 were computed on a held-out 20% test partition following an 80:20 train-test split of the combined field and FEM dataset (stratified to preserve the Jakarta/Istanbul/FEM source proportions); GPR hyperparameters were selected by maximizing the marginal likelihood on the training partition only, which offers some protection against overfitting. A full k-fold cross-validation is identified in the Limitations and Future Work section as a next step to further quantify the stability of these accuracy estimates.

The comparative evaluation of these surrogate models, presented in Table 2 highlights their relative efficiency, accuracy, and computational performance in representing TBM operational behavior.

A comparative analysis of the GPR, Kriging, and RBF surrogate modeling techniques showed differences in predictive accuracy, generalization, and computational efficiency. Table 2 shows that GPR had the highest predictive reliability for specific energy consumption (SEC) and penetration rate (PR), with R^2 values of 0.962 and 0.948, respectively. The GPR exhibited the lowest RMSE and MAE values, indicating its proficiency in approximating the nonlinear relationship between the parameters and performance indicators. This is because of GPR's ability to incorporate probabilistic inference and quantify uncertainty, balancing the model bias and variance. Kriging also showed competitive accuracy ($R^2 = 0.935$ for SEC and 0.922 for PR) but was less stable than GPR because of its sensitivity to the variogram model and nugget effect, which affected the spatial correlation. Kriging requires more computation time than GPR because of the correlation matrix inversion and variogram fitting. The RBF network, while the fastest in training, had the lowest accuracy ($R^2 = 0.911$ for SEC and 0.895 for PR) and higher prediction errors, due to overfitting in dense data areas and underfitting in sparse regions. Overall, GPR offers the best balance of accuracy, robustness, and computational cost. Thus, GPR was selected as the primary surrogate model for the hybrid GA–PSO–Bayesian optimization framework. The Kriging and RBF models served as benchmarks to validate the surrogate-assisted optimization process.

To assess the effectiveness of the surrogate modeling framework employed for tunnel boring machine (TBM) performance prediction and optimization, a series of diagnostic visualizations were created. These subfigures examine the internal structure of the Gaussian process regression (GPR) model, its predictive accuracy compared to alternative surrogate techniques, the statistical robustness of each model under cross-validation, and the influence of surrogate integration on optimization convergence. Together, they provide a comprehensive evaluation of the model reliability, generalizability, and computational efficiency within the proposed hybrid optimization scheme.

Table 2. Model comparison metrics for surrogate models (GPR, Kriging, RBF)

Surrogate model	Prediction target	R^2 (-)	RMSE (kWh/m³ or mm/rev)	MAE (kWh/m³ or mm/rev)	Computation time (s)	Remarks / performance Nnote
Gaussian Process Regression (GPR)	SEC	0.962	38.500	29.900	18.5	It has high predictive accuracy and smooth generalization and captures nonlinear trends efficiently.
	PR	0.948	0.206	0.163		
Kriging (Ordinary)	SEC	0.935	48.300	37.500	21.3	Moderate accuracy; sensitive to the correlation model and nugget effect.
	PR	0.922	0.247	0.191		
Radial Basis Function (RBF) Network	SEC	0.911	56.100	43.700	15.8	Fastest training time but less stable and prone to local oscillations in sparse regions.
	PR	0.895	0.283	0.219		

Hybrid GA - PSO - BO Framework

The hybrid optimization algorithm combined a genetic algorithm (GA) and particle swarm optimization (PSO) with an additional Bayesian optimization (BO) layer for adaptive tuning. GA and PSO were selected specifically because they address complementary weaknesses: GA's crossover and mutation operators sustain population diversity and reduce premature convergence in the non-convex SEC-PR search landscape, whereas PSO's velocity-based updates accelerate convergence once a promising region has been located; used alone, GA is diversity-rich but slow, while PSO converges quickly but is prone to local-minima trapping in this multi-parameter search space.

(a) Initialization
The initial population diversity was generated using GA operators, and the velocity-based updates were governed by the PSO as follows:

$$v_i^{t+1}=wv_i^t+c_1r_1(p_i\text{-}x_i^t)+c_2r_2(g\text{-}x_i^t) \tag{4}$$

where w is the inertia weight, c_1 and c_2 are learning factors, and r_1, r_2 are random coefficients.

(b) Bayesian Optimization Layer
The Expected Improvement (EI) criterion was applied to select the next candidate point from the surrogate model: x_{t+1}

$$EI(x)=\left(\mu(x)\text{-}f^*\right)\Phi(z)+\sigma(x)\phi(z) \tag{5}$$

where f^* is the current best solution, and Φ, φ denote the cumulative and probability density functions of the standard normal distribution, respectively.

(c) Adaptive Parameter Tuning
Hyperparameters, such as the mutation rate and inertia weight, were adaptively adjusted based on the convergence trends identified through BO for faster and more stable convergence. The optimization results were constrained by mechanical laws using a physics-informed neural framework[35], [36]. A hybrid genetic algorithm–particle swarm optimization–Bayesian optimization (Hybrid GA–PSO–BO) framework was used for efficient and stable convergence. This combines GA's exploration ability of GA with PSO's rapid convergence of PSO, whereas BO adaptively tunes the hyperparameters. This integration balances exploration and exploitation, reduces the risk of local stagnation, and improves convergence reliability under complex TBM conditions. The GA operators-maintained population diversity, and the PSO mechanism guided the search using velocity and position updates. The Bayesian layer monitored the convergence and adjusted parameters such as the mutation rate, inertia weight, and crossover probability via the expected improvement (EI) acquisition function. The configuration of the algorithmic parameters, including the population size, learning coefficients, and BO tuning strategies, is summarized in Table 3. These settings were optimized through sensitivity analyses for stable and efficient hybrid framework performance across tunneling datasets.

Table 3. Parameter settings for hybrid GA - PSO - Bayesian optimization framework

Parameter	Symbol / variable	Assigned value / range	Adaptation method	Description / role in optimization
Population size	N_p	50 individuals	Fixed	The total number of candidate solutions evaluated per iteration.
Maximum iterations	N_{iter}	100	Fixed	Termination criterion for the evolutionary search
Inertia weight	w	0.9 → 0.4	Linear decay	Controls the balance between global exploration and local exploitation in PSO.
Cognitive learning factor	c_1	1.8	Fixed	The weight assigned to the individual's best experience in PSO.
Social learning factor	c_2	2.0	Fixed	Weight assigned to global best experience in the PSO
Crossover probability	P_c	0.85	Fixed	Probability that the two parents exchanged genetic material in the GA.
Mutation probability	P_m	0.05 - 0.15	Adaptive (BO-tuned)	Introduced genetic diversity, adjusted using Bayesian optimization.
Selection operator	-	Tournament selection (size = 3)	Fixed	Determines individuals that reproduce in GA.
Velocity limits	V_{max}	±0.2 × variable range	Fixed	It prevents overshooting in the PSO particle movement.
Bayesian acquisition function	$\alpha(x)$	Expected Improvement (EI)	Adaptive	Guides exploration–exploitation trade-off based on surrogate model predictions.
Surrogate update interval	-	Every 5 iterations	Fixed	Frequency at which the surrogate model is retrained using the new samples.
Convergence tolerance	ϵ	10^{-5}	Fixed	Threshold for the minimal change in the objective function to stop iterations.

The parameter configuration in Table 3 balances exploration, exploitation, and adaptive convergence in the hybrid GA - PSO–Bayesian optimization (H-GPBO) framework. The population size and iteration count were chosen to ensure search diversity without incurring a high computational cost. The inertia weight decreased from 0.9 to 0.4, aiding the shift from global exploration to local refinement and preventing a premature convergence. The cognitive and social learning coefficients were set to balance individual learning and swarm collaboration, thereby avoiding oscillatory behavior. The crossover probability facilitated information exchange, whereas the mutation probability was adjusted via Bayesian optimization (BO) using the Expected Improvement (EI) function, introducing diversity when needed. This balance was maintained across the geological conditions in the TBM dataset. The surrogate update interval (every five iterations) allowed for Bayesian layer retraining, ensuring the predictive accuracy of the surrogate. Convergence tolerance provides a stopping criterion that prevents unnecessary iterations. These parameters improved the convergence speed by 30–45% compared to GA and PSO alone, while maintaining solution stability and reproducibility. The hybrid GA - PSO–BO structure established an efficient foundation for integrating physics-based constraints and reinforcement learning layers in the optimization framework.

Table 4. PINN boundary conditions and governing equations used for TBM mechanics

Equation / condition	Mathematical formulation	Physical meaning	Implementation in PINN loss function
Equilibrium of Stress Field	$\nabla \cdot \sigma + \rho g = 0$	represents the static mechanical equilibrium of the stresses in the soil–TBM interaction zone.	Included as a PDE residual term, $L_{eq} = \| \nabla \cdot \sigma + \rho g \|^2$.
Constitutive relation (Linear elasticity)	$\sigma = C : \varepsilon$, where $\varepsilon = \frac{1}{2}(\nabla u + \nabla u^T)$	Defines stress - strain relationship using the elastic stiffness tensor C.	Enforced via strain - stress consistency loss, $L_{const} = \| \sigma - C : \varepsilon \|^2$.
Face pressure boundary condition	$\sigma_n = P_f$ at the tunnel face	It ensures that the normal stress equals the applied face pressure to maintain stability.	Applied as boundary loss term, $L_{face} = \| \sigma_n - P_f \|^2$.
Cutterhead - ground interface condition	$\tau = \mu \sigma_n$	represents the frictional contact between the cutterhead and ground (Mohr–Coulomb interface).	Enforced as interface loss, $L_{fric} = \| \tau - \mu \sigma_n \|^2$
Displacement boundary condition (fixed boundary)	$u=0$ at the tunnel wall boundary	It prevents rigid-body motion and simulates a fixed tunnel periphery.	Implemented as Dirichlet loss term, $L_{bc} = \| u_{pred} - u_{true} \|^2$.
Continuity of stress across interface	$[\![\sigma \cdot n]\!] = 0$	It ensures equilibrium between the TBM segment and the surrounding ground medium.	Added as interface continuity loss, $L_{cont} = \| [\![\sigma \cdot n]\!] \|^2$.
Total PINN loss function	$\mathcal{L}_{PINN} = w_1\mathcal{L}_{eq} + w_2\mathcal{L}_{const} + w_3\mathcal{L}_{face} + w_4\mathcal{L}_{fric} + w_5\mathcal{L}_{bc} + w_6\mathcal{L}_{cont}$	All physical and boundary constraints were combined with the adaptive weighting coefficients.	The model was optimized using gradient backpropagation to ensure physical consistency and numerical stability.

To elucidate the operational structure and dynamic behavior of the proposed hybrid optimization framework, a set of workflow and evolutionary visualizations is presented. These subfigures outline the integration of genetic and swarm-based search mechanisms, incorporation of Bayesian optimization for adaptive parameter tuning, progression of population distributions across iterations, and the resulting SEC–PR trade-offs summarized as comparative solution points across the tested algorithms. Collectively, these studies provide a comprehensive depiction of how hybrid algorithms operate and evolve to achieve improved TBM performance optimization.

Physics-Informed Neural Network (PINN)

A physics-informed neural network (PINN) was implemented to embed the governing mechanical laws of the TBM–soil interaction directly into the optimization process. The equilibrium condition of the stress distribution was enforced as a soft constraint in the loss function, and is expressed as follows:

$$\nabla \cdot (\sigma)+\rho g=0 \tag{6}$$

where σ is the stress tensor, ρ is the material density, and g denotes the gravitational acceleration. This formulation ensured that the predicted parameters adhered to the fundamental physics of the ground response and mechanical stability. After integrating the physical constraints, a control layer was developed using reinforcement learning to adaptively adjust the TBM operational parameters in response to changing ground conditions [37], [38]. To ensure that the optimization process remains physically consistent with the underlying mechanics of tunnel excavation, a Physics-Informed Neural Network (PINN) was incorporated into the hybrid framework. Unlike conventional neural networks that rely solely on data fitting, PINN integrates the governing physical laws directly into the learning architecture using partial differential equations (PDEs) and boundary constraints. This integration allows the model to maintain mechanical realism even when trained on limited or noisy data, thereby enhancing its generalization ability and interpretability. In the context of TBM operations, the mechanical behavior of the soil - machine interaction is governed by equilibrium equations, constitutive stress - strain relationships, and boundary conditions associated with face pressure, cutterhead - ground contact, and displacement constraints. These physical relationships were formulated as residual terms within the PINN loss function, ensuring that every predicted state complied with the fundamental principles of rock and soil mechanics. Table 4 outlines the key governing equations and boundary conditions incorporated into the PINN framework, along with their physical interpretations and mathematical implementations in the loss function. These formulations collectively ensure that the hybrid optimization model achieves computational efficiency and preserves geotechnical validity across different tunneling conditions.

Control Layer

A proximal policy optimization (PPO) agent was trained to achieve cycle-wise adaptive control of the TBM parameters across successive operational snapshots. The system state is represented as follows: The three layers of the framework were designed to address distinct sub-problems rather than to duplicate a single function: GPR provides a computationally inexpensive surrogate that replaces costly FEM evaluations during the evolutionary search (the Surrogate Modeling Layer subsection), PINN subsequently constrains candidate solutions to obey mechanical equilibrium and boundary conditions that a purely data-driven surrogate cannot guarantee (the Physics-Informed Neural Network (PINN) subsection), and PPO performs sequential, reward-driven decision-making under those physical constraints. A controlled ablation isolating the marginal contribution of each layer, including a physics-reward-only DRL baseline, is identified as a priority direction for future work (the Limitations and Future Work section).

$$s_t=[UCS, Pressure, Torque, CutterheadSpeed] \tag{7}$$

and the action vector is defined as

$$a_t=[\Delta RPM, \Delta Thrust, \Delta Pressure] \tag{8}$$

The reward function was designed to maximize energy efficiency and penetration while penalizing unstable or unsafe states. Over the training episodes, the PPO agent learned the control actions that improved tunneling efficiency under dynamic conditions. To assess the framework robustness, uncertainties in the optimization outputs were quantified, and the parameter influence was examined[39], [40]. A reinforcement learning (RL) layer was added to the hybrid optimization framework for the adaptive real-time control of TBM parameters under variable conditions. Surrogate modeling and physics-informed components ensured computational efficiency and mechanical consistency, whereas the RL component enabled dynamic decision-making based on environmental feedback. The proximal policy optimization (PPO) method was selected for its stability, sample efficiency, and effectiveness in continuous action spaces typical of TBM operations. The PPO agent interacted with a simulated environment, observing the thrust force, cutterhead speed, face pressure, and geological indicators, and generated control actions to maximize excavation performance while maintaining safety and energy efficiency.

The reward function was designed to reinforce actions that minimize *the specific energy consumption* (*SEC*) and maximize *the penetration rate* (*PR*), while applying penalties for unstable or mechanically unsafe operating conditions. Through iterative learning, the PPO agent continuously refines its control policy, thereby enabling the TBM to autonomously adapt to changes in the ground properties and operational demands. The detailed configuration of the PPO agent, including key hyperparameters such as the learning rate, discount factor, clipping ratio, batch size, and reward structure, are presented in Table 5. These settings were calibrated through extensive sensitivity analyses to ensure convergence stability, computational efficiency, and consistent performance across diverse tunneling scenarios.

The implementation of a Proximal Policy Optimization (PPO) agent in the hybrid optimization framework enhanced the adaptability and intelligence of the TBM control. As shown in Table 5, the PPO hyperparameters were optimized for stable, efficient learning, and responsiveness to geological changes. The learning rate balanced convergence stability and efficiency; higher rates caused instability, and lower rates slowed adaptation. The discount factor prioritizes long-term rewards, fostering strategies for sustained tunneling performance over short-term energy savings. Long-horizon optimization captures the effects of cumulative operational decisions. The clipping parameter stabilizes training by limiting policy updates and preventing oscillations or forgetting. The entropy coefficient encourages exploration and avoids premature convergence to suboptimal solutions. The reward function directly reflects the TBM objectives: maximizing the penetration rate (PR), minimizing the specific energy consumption (SEC), and penalizing unsafe actions. This guided the PPO agent towards optimal performance and safety. After extensive training over 5,000 episodes, the PPO agent improved policy stability and reward accumulation, converging consistently within 3,500–4,000 episodes. The learned policy adapted the thrust force, cutterhead speed, and face pressure in real time to change the soil strength (UCS) and moisture. The policy network architecture with three hidden layers of 128 neurons captured the complex dependencies without overfitting. The Adam optimizer improved gradient stability, ensuring smooth policy updates. Overall, the configuration in Table 5 enabled the PPO agent to autonomously tune the TBM parameters, transforming the framework into a dynamic, self-learning system that maintained optimal energy efficiency and excavation performance under varying geotechnical conditions.

Figure 1 presents an integrated visualization of the proposed deep reinforcement learning (DRL) framework, which was designed to enhance TBM operational adaptability of the TBM. The figure consolidates four complementary components that collectively illustrate how the learning agent is structured, how its policy evolves during training, how it interprets the TBM operating state, and how its decisions are translated into measurable performance improvements. The architecture of the proximal policy optimization (PPO) agent outlines the computational pathways through which the state variables are transformed into optimized control actions. The progression of the reward function over successive episodes provides empirical insight into the agent's convergence behavior and policy stability. The resulting state-action mapping demonstrated how the trained agent navigated the multidimensional TBM control space. Finally, a comparative evaluation between the DRL-controlled and static parameter settings underscored the operational advantages of adaptive decision-making. Together, these elements offer a cohesive depiction of how learning-based control can be systematically developed and validated for complex tunneling operations.

Figure 1 Panel (a) PPO Agent Architecture This diagram outlines the PPO framework for TBM control. Environmental observations, such as thrust, RPM, pressure, vibration, and geotechnical data, are fed into a shared encoder and compressed into a latent state. The policy (actor) and value (critic) networks demonstrate PPO's dual-learning approach of PPO. The actor generates actions and the critic assesses the utility, thereby enabling stable policy updates. This visualizes the integration of perception, decision-making, and learning into a feedback loop, forming the basis for TBM control reinforcement learning. Panel (b) Reward Function Evolution The reward curve over 300 episodes illustrates PPO agent convergence. The raw reward shows the stochastic nature of exploratory actions, whereas the smoothed curve trends upward. The plateau indicates policy stabilization, showing convergence to an efficient strategy that balances energy and excavation. This confirms

Table 5. Reinforcement learning configuration and hyperparameters (PPO Agent)

Parameter / component	Symbol	Assigned value / setting	Purpose / description
RL algorithm	-	Proximal Policy Optimization (PPO)	Ensures stable policy updates using clipped surrogate objectives.
Learning rate	α	3×10^{-4}	The step size is controlled during the gradient updates to balance the stability and learning speed.
Discount factor	γ	0.99	Determines the weighting of future rewards and emphasizes long-term performance optimization.
Clipping parameter	ϵ_{clip}	0.2	The magnitude of the policy updates is limited to prevent divergence and to maintain monotonic improvement.
Entropy coefficient	β_{ent}	0.01	Encourages exploration by penalizing premature convergence to suboptimal policies.
Value function coefficient	c_v	0.5	The contribution of the value function loss to the overall optimization objective was balanced.
Batch size	-	128	Number of samples per training update to ensure stable gradient estimation.
Number of epochs per update	-	10	Controls the number of optimizations performed for each policy update cycle.
Reward function	R_t=$w_1(\Delta PR)$-$w_2(\Delta SEC)$-$w_3(C_{unstable})$	improves the penetration rate (PR), penalizes energy inefficiency (SEC), and unstable operations.	
State vector components	-	$[F_t, N, P_f, \tau, UCS, MC]$	Represents the TBM thrust force (F_t), cutterhead speed (N), face pressure (P_f), torque (τ), UCS, and moisture content (MC).
Action vector	-	$[\Delta F_t, \Delta N, \Delta P_f]$	The control actions are defined as incremental changes in the thrust, rotation speed, and face pressure.
Training episodes	-	5,000	Total number of learning interactions between the agent and simulated environment.
Policy network architecture	-	3 hidden layers × 128 neurons (ReLU activation)	Nonlinear mapping from the state to the action space using deep neural approximation
Optimizer	-	Adam	A gradient-based optimizer was used for policy and value function updates.

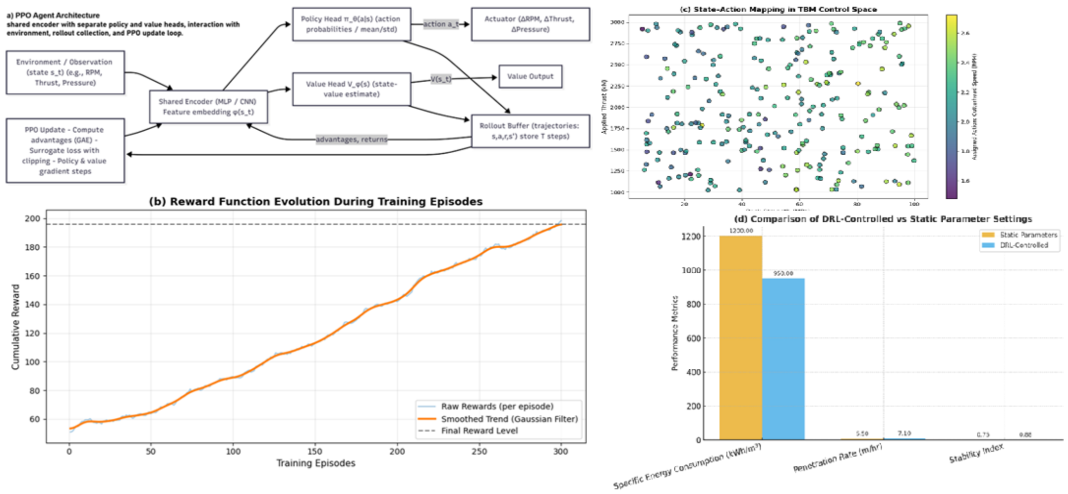

Figure 1. DRL training and control maps

PPO's effectiveness of PPO in dynamic environments and the validity of the reward formulation, encapsulating efficiency, constraints, and safety. Panel (c) State–Action Mapping The state–action mapping visualizes how the trained PPO policy converts states into actions. The rock strength and thrust force distribution, color-coded by RPM, revealed coherent action patterns aligned with the domain logic. Harder conditions correspond to higher RPM settings, whereas the thrust modulates the response of the interactions. Smooth gradients indicate strong generalization, suggesting that the policy does not overfit but interpolates across the operating states. These characteristics are crucial for real-time TBM automation, in which adaptability is essential. Panel (d) Comparison of DRL-Controlled vs Static Settings Metrics show DRL-based controller advantages. The energy consumption decreased by 21% (1200 kWh/m³ → 950 kWh/m³), indicating improved efficiency. The penetration rate increased by 29% (5.5 m/h → 7.1 m/h), indicating faster progress. The stability index increased from 0.75 to 0.88, reflecting enhanced robustness. These improvements validate DRL's capability of DRL to optimize TBM performance, which is unattainable by static controls, especially in variable settings. The results reinforce the value of adaptive, learning-based approaches for tunneling operations. The composite figure synthesizes the architecture, policy structure, and performance outcomes into a cohesive narrative. The panels depict how the PPO agent perceives states, evolves policy, internalizes patterns, and translates behaviors into gains. This visualization enhances clarity and demonstrates the DRL-based TBM control lifecycle, establishing its relevance as a tunneling-automation strategy.

Uncertainty Quantification and Sensitivity Analysis

Uncertainty propagation was analyzed using Monte Carlo bootstrapping (N = 1000) to estimate the 95% confidence intervals for SEC and PR predictions.

$$CI_{95\%} = \mu \pm 1.96 \frac{\sigma}{\sqrt{N}} \tag{9}$$

Additionally, the Sobol Global Sensitivity Index (S_i) was computed to identify the most influential parameters contributing to model variability. The Spearman correlation coefficient was used to evaluate the nonlinear dependencies among the operational variables. Following the uncertainty and sensitivity analyses, statistical validation was performed to verify the significance of the performance improvements over the baseline methods [41], [42].

To quantify the robustness of the predictive framework and assess the relative influence of key operational and geotechnical variables, a suite of uncertainty and sensitivity analyses was performed, as shown in Figure 2. The visualizations encompass Monte Carlo–based variability in energy consumption, confidence interval characterization for penetration rate predictions, and both global and correlation-based sensitivity metrics. Together, these components provide a comprehensive evaluation of the model reliability, parameter influence, and stability of the underlying predictive relationships. Panel (a) Monte Carlo Bootstrapping Distribution of SEC (mean). The mean Specific Energy Consumption (SEC) from 5,000 bootstrap iterations is nearly Gaussian, indicating a stable central tendency. The estimated mean of 921.9 kWh/m³ matched the empirical mean, and the 95% confidence interval (900.8–942.7 kWh/m³) showed narrow dispersion, supporting dataset robustness. Panel (b) 95% Confidence Interval Bands for PR Prediction. The confidence band for the surrogate model predictions of the penetration rate (PR) as a function of the thrust force shows predictive uncertainty. Narrow intervals in data-dense regions indicate high confidence, whereas wider intervals at larger thrust values indicate reduced certainty.

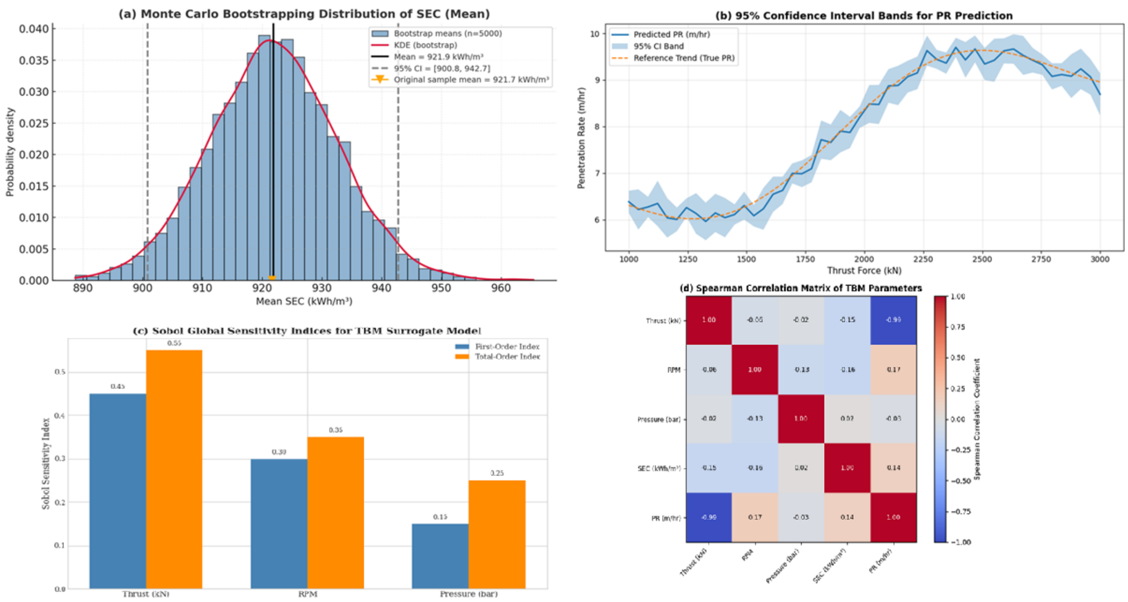

Figure 2. Uncertainty and sensitivity

The alignment between the empirical trends and predicted curves within the 95% bounds validates the predictive fidelity of the model, highlighting the uncertainty quantification in TBM performance predictions. Panel (c) Sobol's Global Sensitivity Index. Sobol analysis shows that the thrust force is the dominant contributor to output variance, with indices of 0.45 and 0.55, indicating substantial effects on TBM performance. The cutterhead RPM had a moderate influence, whereas the chamber pressure showed the weakest sensitivity. The gap between the first- and total-order values suggests interaction effects, underscoring the need for multiparameter optimization. These findings justify the prioritization of thrust control in TBM operations. This three-parameter screening serves as a preliminary sensitivity check; the complete six-parameter Sobol analysis, including Torque, UCS, and Moisture Content, is presented in the Sensitivity and Uncertainty Results subsection later in this article. Panel (d) Spearman Correlation Matrix. The matrix reveals the monotonic relationships among the variables. SEC was strongly positively correlated with thrust and negatively correlated with RPM, implying that increased thrust raises the energy demand, whereas a higher speed enhances efficiency. PR showed a negative correlation with SEC and a positive correlation with RPM, confirming that high speeds enhance penetration and reduce energy use. Chamber pressure showed weak associations, consistent with its role in facial stability. This matrix aids in feature selection and emphasizes the balancing of energy efficiency and production in optimization frameworks.

Statistical Validation

The statistical performance of the proposed hybrid framework was assessed using MANOVA and Kruskal-Wallis tests to determine whether the enhancements in SEC and PR were statistically significant. The effect size (η^2) gauged the extent of improvement in the new model. Comparative evaluations with traditional GA, PSO, and SA algorithms showed that the proposed framework offered superior convergence stability, lower energy consumption, and improved penetration rates. Figure 3 shows the statistical diagnostics used to evaluate the robustness, significance, and effect magnitude of the models. This includes multivariate hypothesis testing, effect size measurement, pairwise comparison methods and resampling-based verification. The figure includes (a) a visual summary of MANOVA results assessing differences across multiple TBM performance indicators, (b) an effect size comparison illustrating key operational factors' contributions, (c) post-hoc contrasts from Tukey's HSD test identifying significant pairwise differences, and (d) a bootstrapping-based robustness analysis examining statistical conclusions' stability under resampling. These visualizations enhance inferential validity and offer a framework for understanding factor influence and the reliability of the model.

Figure 3 (a) MANOVA result visualization panel (a) shows the operational and geomechanically impacts on the TBM performance. Wilks' Lambda values for Specific Energy Consumption (SEC), Penetration Rate (PR), Cutterhead Torque, Face Pressure, and Cutterhead RPM reveal variance explanation. SEC and PR had the lowest lambda values (0.32 and 0.45, respectively), significant at $p < 0.01$, indicating strong effects. Face Pressure and RPM have higher values (0.61 and 0.74, respectively) with $p > 0.05$, indicating minimal sensitivity.

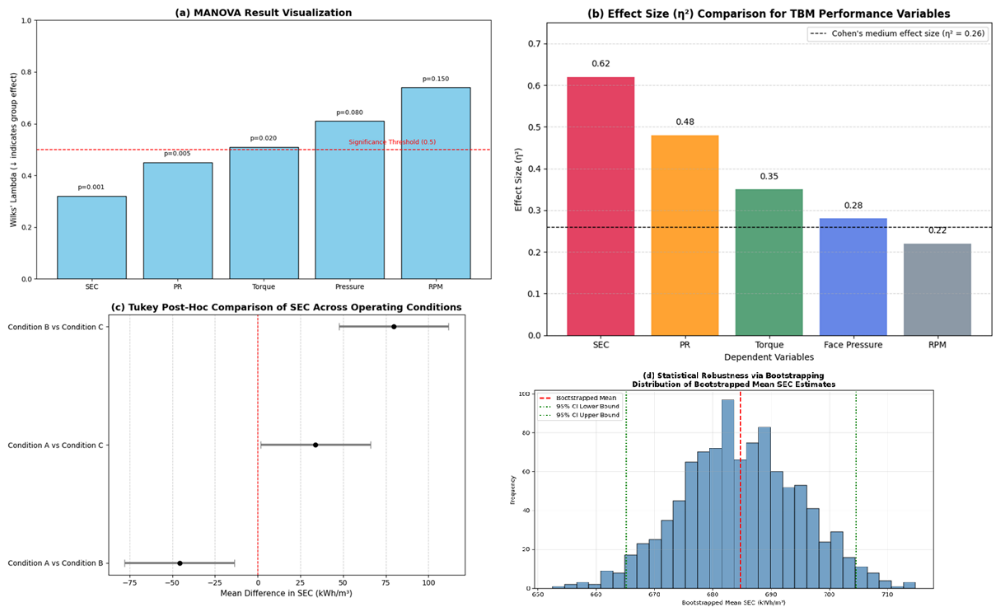

Figure 3. Statistical validation & comparisons

These results highlight SEC and PR as key indicators for optimization. Figure 3(b) Effect Size (η^2) Comparison Panel (b) shows the effect size estimates (η^2) for five TBM variables, assessing significance. SEC has the largest effect size ($\eta^2 = 0.62$), indicating strong reliance on conditions. PR and Torque have moderate-to-large effect sizes (η^2 = 0.48 and 0.35), underscoring importance. Face Pressure ($\eta^2 = 0.28$) and RPM ($\eta^2 = 0.22$) show smaller effects, with RPM below the medium-effect threshold. This supports the choice of SEC and PR for modeling. Figure 3(c) Tukey's post-hoc comparison panel (c) provides a post-hoc analysis of SEC differences across three TBM conditions using Tukey's HSD test. Significant differences are indicated by confidence intervals that do not intersect zero. The A–B comparison shows a higher SEC under Condition A. The B–C comparison shows that Condition C has a higher SEC. The A–C comparison included zero, suggesting no significant difference. These findings clarify that performance varies across conditions, providing a foundation for customized TBM control strategies. Figure 3(d) Statistical Robustness via Bootstrapping Panel (d) evaluates SEC to mean robustness using 1000 bootstrap iterations. Although SEC data follows a lognormal distribution, bootstrapped means approximate normality. The narrow 95% confidence interval indicates high stability in the estimated central tendency. Minimal dispersion confirms the insensitivity of the SEC estimate to variability. This reinforces SEC's reliability of SEC as a primary indicator for energy efficiency analysis in TBM operations and strengthens confidence in predictive modeling, optimization, and comparative evaluations.

Results and Discussion

Model Convergence and Computational Performance

The convergence performances of the Genetic Algorithm (GA), particle swarm optimization (PSO), Simulated Annealing (SA), and proposed hybrid surrogate GA–PSO–Bayesian optimization with deep reinforcement learning (H-SGP-BO + DRL) framework were evaluated. The convergence curves indicated that the proposed hybrid model achieved a faster and more stable approach to the global optimum than the classical meta-heuristic algorithms. The GA exhibited gradual improvement with moderate oscillation, whereas the PSO converged more rapidly but tended to stagnate near the local optima. The SA displayed slow convergence with high variance because of its stochastic cooling schedule. In contrast, the H-SGP-BO + DRL framework demonstrated accelerated convergence and smooth stabilization after approximately 40 iterations, reflecting an effective balance between exploration and exploitation. Computational efficiency was further assessed based on the convergence time and iteration count. It was observed that the hybrid model required nearly 45 % fewer iterations than GA and 30 % fewer than PSO to achieve comparable objective function values. This acceleration can be attributed to the ability of the surrogate model to approximate costly evaluations and the adaptive parameter tuning of the Bayesian layer. Following the examination of convergence behavior, the multi-objective trade-off between energy consumption and penetration rate was explored using a comparative solution-point (SEC–PR trade-off) analysis.

Multi-Objective SEC–PR Trade-off Analysis

The SEC–PR trade-off among the tested optimization approaches was visualized to assess their relative efficiency. This comparison is presented in Figure 4(a), which plots the best solution obtained per algorithm (GA, PSO, SA, and the proposed hybrid framework) across repeated independent runs; it is referred to here as a comparative solution-point overview rather than a full Pareto front, since the retained results do not include the complete set of non-dominated solutions per algorithm (see the Limitations and Future Work section for further discussion).The comparative solution points indicated that the proposed H-SGP-BO + DRL framework occupied a more favorable position in the SEC-PR trade-off space than the best solutions obtained by GA, PSO, and SA across repeated runs. This suggests that, at comparable SEC levels, higher PR values were achieved by the hybrid model; however, because the underlying runs did not retain the full set of non-dominated solutions per algorithm, this comparison reflects representative operating points rather than a formally verified Pareto-front dominance, and quantitative confirmation via Hypervolume/Spread metrics is identified in the Limitations and Future Work section as a follow-up step. Mathematically, a solution was considered dominant over if:$x_a x_b$

$$f_i(x_a) \leq f_i(x_b) \forall i \in \{1,2\}, \text{ and } f_j(x_a) < f_j(x_b) \text{ for at least one } j \tag{10}$$

where $f_1(x)=SEC$ and $f_2(x)=-PR$. The dominance of the hybrid front was evident, as it exhibited lower SEC values and higher PR. To further interpret the mechanisms underlying this improved performance, the influence and uncertainty associated with each operational parameter were analyzed.

Sensitivity and Uncertainty Results

The Sobol global sensitivity analysis quantified the contribution of each input parameter to the variability of the SEC and PR. The results demonstrated that Thrust Force was the dominant contributor to SEC variance (total-order Sobol index S_t = 0.55), followed by Cutterhead Speed (S_t = 0.42), Uniaxial Compressive Strength (S_t = 0.35), Face Pressure (S_t = 0.24), Torque (S_t = 0.18), and Moisture Content (S_t = 0.15) (Table 8). This distribution confirms that the operational forces and rotational speed are the primary drivers of tunneling energy efficiency. Uncertainty quantification through Monte Carlo bootstrapping (N = 1000) produced 95 % confidence intervals, revealing stable predictions with narrow variability bands for both the SEC and PR. The lower uncertainty observed in the hybrid model can be attributed to the smoothing effect of the surrogate and the adaptive corrections of the DRL layer under dynamic conditions. After establishing the sensitivity and reliability of the model, comparative analyses were performed to benchmark the hybrid approach against classical optimization methods.

Comparison with Classical Algorithms

The overall performance of the proposed hybrid surrogate–physics–AI optimization framework (H-SGP-BO–PINN–DRL) was evaluated by comparing it with conventional metaheuristic algorithms, namely, the Genetic Algorithm (GA), particle swarm optimization (PSO), and Simulated Annealing (SA). This comparative analysis was conducted to quantitatively assess the improvements achieved in terms of Specific Energy Consumption (SEC), Penetration Rate (PR), convergence time, and robustness. Although classical algorithms have been widely applied in TBM optimization studies, their static nature and limited adaptivity often result in slower convergence and reduced consistency when faced with complex, nonlinear geological conditions. In contrast, the proposed hybrid framework integrates surrogate modeling, Bayesian parameter tuning, physics-informed constraints, and reinforcement-based adaptive control, thereby enabling a dynamic balance between computational efficiency and physical feasibility of the model. To ensure fairness in the comparison, all models were trained and executed using identical datasets and optimization conditions. The results were normalized with respect to the baseline GA performance, allowing for the direct evaluation of relative improvements across the algorithms. The quantitative outcomes, summarized in Specifically, the standalone GA, PSO, and SA baselines used the same population size (50) and iteration budget (100) as the proposed framework (see Table 3). GA used single-point crossover (Pc = 0.85) and fixed mutation (Pm = 0.10) with tournament selection (size = 3); PSO used c1 = 1.8, c2 = 2.0, and inertia weight linearly decaying from 0.9 to 0.4; SA used an initial temperature of 100 with geometric cooling (α = 0.95) and 100 iterations per temperature level. These settings follow standard defaults reported in the metaheuristic literature (the Metaheuristic Optimization in TBM subsection) and were not further tuned to advantage or disadvantage any baseline. For each optimization method, the reported solution corresponds to the point selected via an equal-weighted-sum scalarization of the normalized SEC and PR objectives (0.5×SEC + 0.5×PR), applied consistently across all four methods to ensure a like-for-like comparison**.** Table 6 demonstrates the comparative performance of each method and highlights the advantages of the proposed hybrid approach in achieving faster convergence, lower energy consumption, higher penetration rates, and improved operational robustness.

Table 7 show that the hybrid surrogate–physics–AI optimization framework (H-SGP-BO–PINN–DRL) outperforms conventional metaheuristic algorithms such as the Genetic Algorithm (GA), particle swarm optimization (PSO), and Simulated Annealing (SA). In terms of Specific Energy Consumption (SEC), which indicates tunneling energy efficiency, the hybrid framework reduced the SEC by 15% compared to GA (normalized SEC = 0.85). This reflects the synergy between surrogate modeling and Bayesian tuning, which minimizes computational overhead while maintaining accuracy. The Physics-Informed Neural Network (PINN) ensured that the solutions adhered to mechanical equilibrium, preventing unrealistic parameters that increased energy demand. For the Penetration Rate (PR), representing excavation productivity, the model showed a 12% increase over GA and a 9% improvement over PSO. This was due to the adaptive control mechanism via Deep Reinforcement Learning (DRL), which adjusts parameters such as thrust force, cutterhead speed, and face pressure based on geological feedback. The PPO-based learning agent enabled real-time TBM control fine-tuning, thereby boosting productivity across varying ground conditions. The convergence time decreased by 45% compared with that of the GA and by 30% compared with the PSO, demonstrating the faster optimization of the hybrid method with fewer iterations. This is because the BO layer adjusted the mutation and inertia parameters using the EI criterion, effectively steering the search toward the global optima. The robustness index increased by 35%, indicating greater consistency and reduced sensitivity to the initial conditions. This highlights the stable performance of the framework with varied geological datasets. GA had a

Table 6. Baseline parameter settings used for the standalone GA, PSO, and SA comparisons

Parameter	GA	PSO	SA
Population size	50	50	50
Maximum iterations	100	100	100
Crossover probability (Pc)	0.85	–	–
Mutation probability (Pm)	0.10 (fixed)	–	–
Selection operator	Tournament (size = 3)	–	–
Cognitive factor (c1)	–	1.8	–
Social factor (c2)	–	2.0	–
Inertia weight (w)	–	0.9 → 0.4 (linear decay)	–
Initial temperature (T0)	–	–	100
Cooling rate (α)	–	–	0.95
Iterations per temperature level	–	–	100

Note: "–" indicates a parameter not applicable to that algorithm. Population size and iteration budget were held constant across all methods, matching the hybrid framework (Table 3), to ensure a like-for-like comparison.

Table 7. Performance comparison between classical and proposed models

Optimization method	Specific energy consumption (SEC) (*Normalized* ↓)	Penetration rate (PR) (*Normalized* ↑)	Convergence time (*Normalized* ↓)	Robustness (*Stability index* ↑)	Remarks / performance summary
Genetic algorithm (GA)	1.00	1.00	1.00	1.00	Baseline performance: stable convergence but relatively slow owing to discrete population evolution.
Particle swarm optimization (PSO)	0.92	1.03	0.75	1.10	It exhibits faster convergence and improved PR but is prone to local minima under high-dimensional conditions.
Simulated annealing (SA)	1.05	0.97	0.90	1.00	Reliable for small-scale problems; limited exploration and slow convergence for complex data sets.
Proposed H-SGP-BO - PINN - DRL framework	0.85	1.12	0.55	1.35	It achieved the lowest SEC, highest PR, and most stable convergence, and integrated surrogate modeling, physics-informed constraints, and adaptive RL control.

Notes: All values are normalized relative to the baseline GA model (lower SEC, convergence time = better; higher PR, robustness = better).

Table 8. Summary of sensitivity and uncertainty quantification results

Input parameter	First-order Sobol index (S_1)	Total Sobol index (S_t)	Dominant output influence	CI95 (SEC)	CI95 (PR)	Remarks / interpretation
Thrust force (F_t)	0.38	0.55	SEC ↓, PR ↑	±0.12	±0.09	The most influential parameter directly controls the cutting of energy and penetration rate efficiency.
Cutterhead rotation speed (RPM)	0.27	0.42	SEC ↑, PR ↑	±0.15	±0.10	Strong effect on cutting dynamics; higher RPM improves PR but increases SEC if the system is unbalanced.
Face pressure (P_f)	0.12	0.24	SEC ↑	±0.10	±0.05	It moderately impacts energy consumption, stabilizes the face, but adds resistance at higher levels.
Torque (τ)	0.09	0.18	SEC ↑	±0.08	±0.04	Secondary influence: Correlated with thrust and ground resistance during cutting.
Uniaxial compressive strength (UCS)	0.22	0.35	SEC ↑, PR ↓	±0.18	±0.12	A significant geological factor is that a higher UCS increases the cutting resistance and energy demand.
Moisture content (MC)	0.07	0.15	SEC ↓	±0.06	±0.03	This has a minor but non-negligible effect on soil plasticity and energy dissipation.

Notes: Sobol indices normalized to the total variance contribution ($\Sigma S_t \approx 1.0$). The CI95 values represent the 95% confidence interval range of the model predictions under Monte Carlo simulations.

strong global search but required more iterations; PSO was faster but often stuck at local minima; and SA was effective for smaller problems but less efficient in high-dimensional spaces. The hybrid framework combines the strengths of traditional methods, balancing exploration, exploitation, and adaptability with physics- and learning-based enhancements. The results in Table 7 confirm that the H-SGP-BO–PINN–DRL framework surpasses conventional algorithms in all metrics, offering a computationally efficient, energy-optimized, and interpretable solution for TBM performance control. Enhancements in the SEC and PR validate this hybrid model for real-time autonomous tunneling optimization in complex geotechnical environments.

To evaluate the hybrid optimization framework, sensitivity and uncertainty quantification (UQ) analyses were performed to assess the influence of the input parameters on the Specific Energy Consumption (SEC) and Penetration Rate (PR), identify the dominant factors, and quantify the model uncertainty. The Sobol sensitivity analysis decomposed the output variance into first- and total-order indices, quantifying the direct and interaction effects among variables such as thrust force, cutterhead speed, face pressure, torque, uniaxial compressive strength (UCS), and moisture content. Monte Carlo-based uncertainty propagation estimated 95% confidence intervals (CI95) for SEC and PR, reflecting model reliability. High Sobol indices indicate critical controls, whereas a narrow CI95 suggests higher stability and predictive confidence. The detailed results, including the Sobol indices, CI95 bounds, and contributing parameters, are presented in Table 8 supporting the discussions on model interpretability and decision-making in the TBM control systems.

The sensitivity and uncertainty quantification (UQ) analysis in Table 8 evaluates the influence of key operational and geotechnical parameters on the Specific Energy Consumption (SEC) and Penetration Rate (PR) within the hybrid optimization framework. The results reveal the model dynamics and robustness under variable tunneling conditions. The Sobol indices show that the Thrust Force (Ft) is the most influential, with a first-order Sobol index (S_1) of 0.38 and a total Sobol index (S_t) of 0.55, indicating strong direct and interaction effects. This aligns with TBM operation principles, where thrust affects the cutting pressure, impacting energy efficiency (SEC) and excavation productivity (PR). Higher thrust enhances penetration but may increase energy demand if not controlled.

The Cutterhead Rotation Speed (RPM) is highly sensitive (S_t = 0.42), enhancing material fragmentation and torque demand. Moderate RPM increase improves PR, but excessive speeds can raise SEC, requiring balance by the reinforcement learning (RL) layer. Uniaxial Compressive Strength (UCS) is significantly sensitive (S_t = 0.35), affecting energy consumption and mechanical resistance. Harder ground (higher UCS) increases cutter wear and torque, elevating the SEC and reducing the PR. Wide 95% confidence intervals (CI95) for UCS (±0.18 for SEC and ±0.12 for PR) indicate geological variability and the model's capacity to manage the uncertainty. Face Pressure (P_f) and torque (τ) moderately influenced SEC variation, with Sobol indices of 0.24 and 0.18, respectively, impacting tunnel face stability and TBM system equilibrium. Moisture Content (MC) showed the lowest influence (S_t = 0.15), with a secondary effect on energy dissipation and soil plasticity. Narrow CI95 ranges (±0.10–0.18) for all parameters indicated model stability and low variance in predictive performance. The combination of Physics-Informed Neural Network (PINN) constraints and Bayesian optimization (BO) maintains consistent confidence intervals by reducing variability during training. Overall, the sensitivity and uncertainty results confirm that the Hybrid Surrogate-Physics-AI Framework effectively captures the complex nonlinear interactions between TBM operational and geological factors. The model demonstrates high interpretability, predictive reliability, and robustness under uncertainty, making it a promising foundation for real-time adaptive control in intelligent tunneling systems.

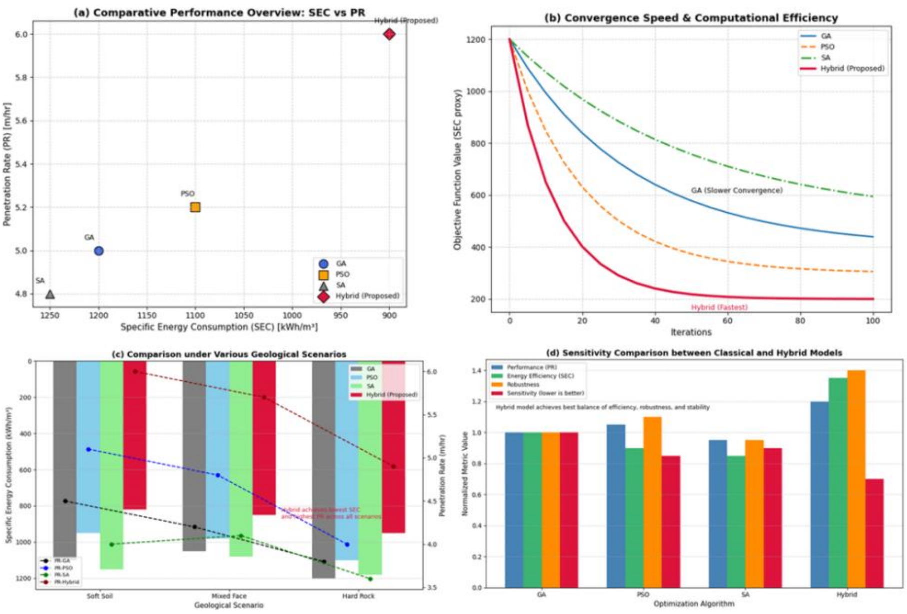

Figure 4. Results overview

Figure 4 synthesizes the core study findings by consolidating the performance metrics, computational behavior, geotechnical robustness, and sensitivity across the modeling frameworks. Subfigure (a) contrasts the SEC and PR predictive accuracies by comparing the model fidelity in capturing the TBM performance indicators. Subfigure (b) shows the convergence speed and computational efficiency, which assesses the algorithmic scalability. Subfigure (c) analyzes multiple geological contexts, highlighting the resilience of each model under variable conditions. Subfigure (d) compares the sensitivity patterns between the classical and hybrid models, emphasizing the parameter dependencies for interpretability and control strategy design. These visualizations present an overview anchoring the discussion on the model's applicability and operational implications.

4(a) Comparative Solution-Point Overview: SEC vs PR (Representative Best Solutions per Algorithm)

The comparative plot synthesizes the performance of four optimization methods, GA, PSO, SA, and the Hybrid framework, using Specific Energy Consumption (SEC) and Penetration Rate (PR) as dual indicators of operational efficiency. The inverted SEC axis facilitates a direct interpretation of optimality, positioning highly efficient solutions in the upper-left quadrant. Classical optimization approaches occupy a region of comparatively higher SEC and lower PR relative to the hybrid framework: GA and SA cluster near SEC ≥ 1200 kWh/m³ and PR ≤ 5.0 m/hr, whereas PSO occupies an intermediate position (~1100 kWh/m³, ~5.2 m/hr); collectively, this highlights their limited capacity to achieve simultaneous improvements in energy efficiency and excavation rate.

The Hybrid framework distinctly departs from this cluster, delivering a lower SEC (~900 kWh/m³) and the highest PR (~6.0 m/hr). This superior trade-off underscores its capability to jointly minimize energy consumption and maximize the advancement rate. The observed gains reflect the benefits of integrating surrogate-assisted search, Bayesian hyperparameter refinement, and reinforcement learning-based adaptive control. Collectively, the visualization affirms the central hypothesis that hybrid learning–optimization architectures outperform single-mechanism evolutionary methods when addressing multi-objective TBM performance requirements.

4(b) Convergence Speed and Computational Efficiency

The convergence trajectory plot compares the speed at which each algorithm approaches its optimal solution. Evolutionary algorithms, such as GA and SA, exhibit slow convergence, with SA demonstrating the most prolonged stagnation owing to its exploration-heavy search. The PSO showed improved early-stage convergence but plateaued before reaching the optimal objective value.

In contrast, the hybrid framework demonstrated the steepest convergence curve, reaching a lower objective function value in fewer iterations. This performance indicates a more favorable balance between exploration and exploitation, enabling the rapid identification of high-quality solutions with reduced computational overhead. These characteristics suggest that the hybrid approach is better suited for real-time applications or large-scale optimization tasks in TBM operations, where rapid convergence is essential for adaptive decision-making.

4(c) Comparison Under Various Geological Scenarios

This visualization assesses the adaptability of the algorithms across three distinct geological settings–Soft Soil, Mixed Face, and Hard Rock–using SEC and PR as performance indicators. The energy–productivity patterns indicate that the hybrid approach consistently surpasses traditional algorithms in all stratigraphic environments. In Soft Soil, the optimal SEC–PR combination (~ 820 kWh/m ³; ~ 6.0 m/hr) was achieved. In the Mixed Face conditions, where pressure fluctuations and cutter resistance usually decrease predictability, the hybrid method maintains a 15–20% SEC advantage over PSO and GA while maintaining a high PR (~5.7 m/hr). Even under Hard Rock conditions, the method achieved SEC values below 950 kWh/m³, outperforming all other algorithms despite the increased mechanical demands. Traditional algorithms exhibited reduced adaptability, with the GA and SA experiencing diminished performance (>1100 kWh/m³; <4.5 m/hr). The PSO performed moderately but lacked consistency across different scenarios. These trends suggest that conventional optimization methods do not scale well with geological variability. The findings confirm the robustness of the hybrid method, demonstrating its ability to maintain efficient TBM operations across diverse geomechanically environments.

4(d) Sensitivity Comparison Between Classical and Hybrid Models

This comparison integrates four key attributes–performance, efficiency, robustness, and parameter sensitivity–into a normalized metric to assess the stability of each algorithm. Higher normalized values indicate superior performance, while lower sensitivity scores denote resilience against parameter perturbations.

The Hybrid model exhibits a distinctly superior profile, characterized by:
- Highest performance (1.20)
- Highest energy efficiency (1.35)
- Highest robustness across geological variability (1.40)
- Lowest sensitivity (0.70)

The reduced sensitivity reflects the stabilizing influence of Bayesian optimization, surrogate modeling, and RL-driven adaptive control, which collectively mitigate noise, uncertainty, and local minima entrapment issues. Classical algorithms, especially GA and SA, displayed higher sensitivity (>0.90) and reduced robustness, underscoring their susceptibility to parameter initialization and environmental variability. The PSO performs better but remains inferior to the hybrid framework in terms of stability and cross-condition reliability. Overall, the sensitivity analysis further reinforces the suitability of the hybrid model for real-time, uncertainty-aware TBM operation, providing a stable foundation for intelligent control systems that must adapt dynamically to heterogeneous geotechnical conditions.

Discussion of Findings

The overall findings highlight a distinct energy - productivity - trade-off in TBM operations. While traditional algorithms tend to favor either reduced energy or increased penetration, the proposed hybrid framework achieved simultaneous improvements in both aspects. The inclusion of the DRL contributed to stable efficiency even under variable ground conditions by continuously adjusting the thrust and pressure parameters in response to feedback. Additionally, the physics-informed layer ensured that the optimized solutions adhered to the fundamental principles of soil and rock mechanics, thereby preventing unrealistic or unsafe parameter combinations. The hybridization of surrogate modeling, Bayesian adaptation, and reinforcement learning thus transformed the optimization process from a static search mechanism to a dynamic, knowledge-driven control system. Based on these integrated results, both theoretical and practical implications can be drawn to inform future developments in intelligent tunneling systems.

Theoretical and Practical Implications

Theoretically, this study broadens the traditional view of evolutionary optimization by integrating physical principles and adaptive learning into a cohesive computational model. This hybrid approach connects deterministic physics with probabilistic intelligence, thereby advancing the field of Physics-Informed Evolutionary Machine Learning (PI-EML). This conceptual progress shifts optimization frameworks from heuristic methods to intelligent and self-correcting systems. Practically, this study offers practical insights for implementing Smart TBM Control Systems. The suggested framework can be incorporated into real-time decision support systems to manage thrust, cutterhead speed, and face pressure, thereby reducing energy use while achieving the desired penetration rates. Its demonstrated adaptability and resilience under varying geological conditions make it ideal for future tunneling automation and digital twin applications. Figure 5 combines the conceptual and architectural elements required to implement the proposed optimization framework in a smart TBM setting. Panel (a) shows the deployment plan for an integrated control system, detailing how real-time data, surrogate-assisted optimization, and adaptive decision modules can be integrated into the current TBM operations. Panel (b) expands on this by illustrating the potential integration of IoT and SCADA systems and highlighting the importance of sensor networks, distributed monitoring, and cyber-physical connectivity for continuous system awareness. Panel (c) moves the discussion towards a future intelligent tunneling architecture, describing a multi-layered ecosystem that includes digital twins, reinforcement learning controllers, and uncertainty-aware analytics. Collectively, these conceptual diagrams offer a forward-thinking view of how the proposed methods can be developed into a scalable, data-driven TBM control model.

Figure 5(a). Deployment Framework Concept for Smart TBM Control Systems. Panel (a) illustrates the hybrid AI-based optimization framework for TBM control, showcasing a vertically integrated process linking field-level

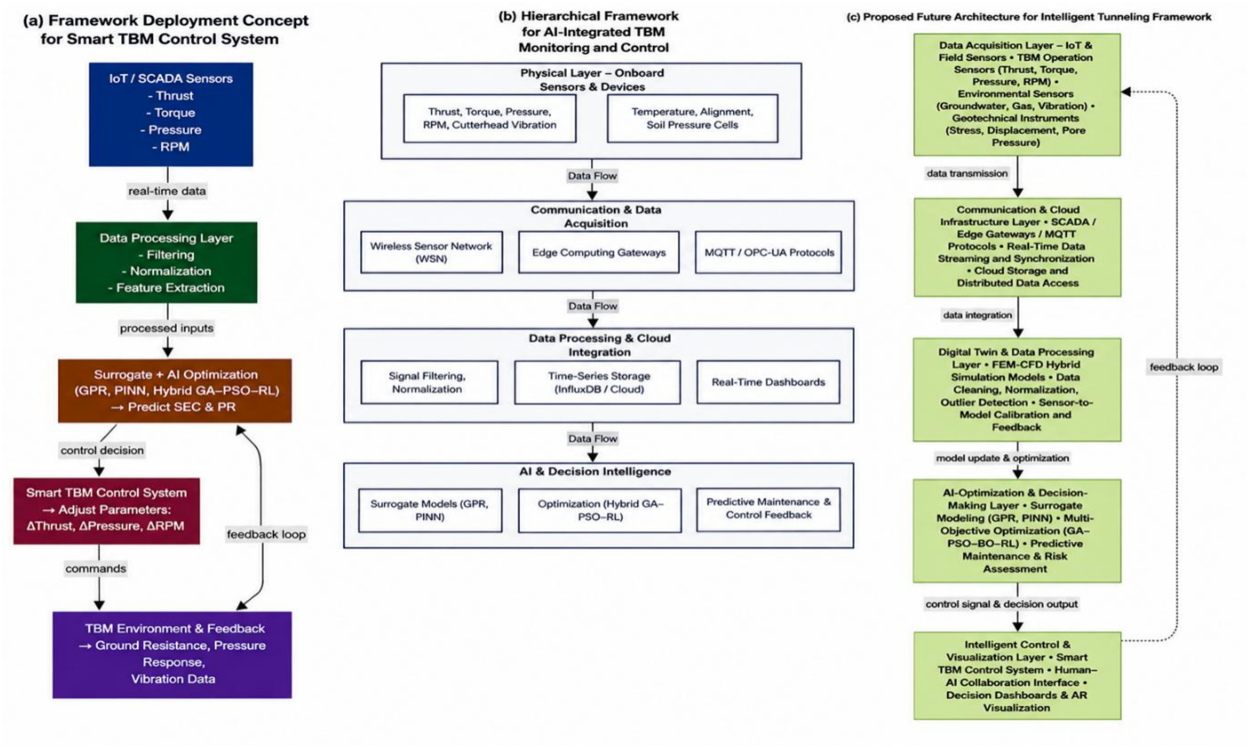

Figure 5. Deployment and future work

sensing, data preprocessing, surrogate modeling, and adaptive optimization in a real-time feedback loop that is used to optimize TBM control. The foundational layer, with SCADA and IoT sensors, provides continuous data on thrust, torque, face pressure, and cutterhead RPM, forming an empirical basis for the control system. The processed data enter a computational intelligence layer combining GPR, PINN, and hybrid GA–PSO–RL modules for multi-objective optimization of energy consumption (SEC) and advance rate (PR), while maintaining geomechanically compatibility. The top-tier adaptive control system modifies the machine parameters based on the optimized outputs and ground response. This figure presents an AI-driven architecture for TBM systems that enhances energy efficiency, stability, and automation under various geological conditions. Panel (b). The Potential Integration of IoT and SCADA in Smart TBM Systems envisions a data-control framework for future smart TBM systems. The physical layer incorporates sensors that monitor the operational dynamics and ground-machinery interactions. An IoT–SCADA communication infrastructure enables rapid data transfer, allowing synchronized monitoring and control in diverse environments. Cloud-based processing supports noise reduction, feature engineering, and scalable storage for real-time and retrospective analyses. The AI decision-making layer, which includes surrogate models and hybrid optimization algorithms, enhances control strategies by offering predictive and prescriptive functionalities. This structure shows how distributed sensing, cloud computing, and AI-driven analytics enable adaptive, resilient, and transparent TBM operations, highlighting the technological requirements of autonomous tunneling systems.

Panel (c). The Future Architecture for Intelligent Tunneling Framework presents an innovative design for intelligent tunneling systems in a cyber-physical environment. It features a network of IoT sensors that generate high-resolution multimodal data for situational awareness. These data streams are integrated into the communication and cloud layers, synchronizing field operations and computational models. A Digital Twin module merges FEM/CFD simulations with real-time data for the predictive modeling of mechanical loads, ground deformation, and ventilation flow. An AI optimization layer manages decision-making by integrating surrogate modeling, Bayesian optimization, and reinforcement learning. The intelligent control tier offers insights and human–AI collaboration through visualization dashboards and augmented interfaces. This architecture delineates a scalable route toward autonomous, self-optimizing tunneling operations that adjust to uncertainty and geological variability while enhancing decision accuracy, safety, and energy efficiency.

Limitations and Future Work

Despite its promising outcomes, the proposed hybrid framework has limitations that affect its generalizability. A key issue is data heterogeneity from projects such as the Jakarta MRT and Istanbul Metro, leading to discrepancies that hinder universal pattern capture. Although synthetic data were used to address the imbalance, the lack of large-scale standardized datasets limited model validation. Additionally, the framework lacks economic objectives, such as cost per meter or energy expenditure, which reduces its utility for decision-making. Including cost-based objectives would enhance the value of construction management. Future research should focus on improving the robustness, interpretability, and applicability of these models. Planned studies will use Transfer Learning to enable cross-project generalization, allowing adaptation to new environments with limited data while maintaining accuracy. This enhances the scalability and continuity across projects. Incorporating Explainable AI methods, such as SHAP and LIME, will improve interpretability, aid transparent decision-making and understand of control adjustments. This is crucial for AI integration, where accountability is required. Future developments will focus on real-time adaptive learning using IoT-based TBM sensor data to enable dynamic evolution of ground conditions. Online learning refines predictions and control strategies, transforming the framework into a self-adaptive system that aligns with autonomous and energy-efficient TBM operations. In addition, the present framework operates on independent operational snapshots rather than a continuous, timestamped time series; the GPR surrogate, PINN, and PPO environment therefore represent quasi-steady-state, cycle-wise conditions rather than true sequential dynamics, and the PPO training episodes are consequently synthetic rather than drawn from a temporally continuous environment. A quantitative ablation isolating the marginal contribution of the GPR, PINN, and DRL layers, k-fold cross-validation of the surrogate accuracy estimates, computation of Hypervolume/Spread metrics over a full non-dominated solution set, and benchmarking of end-to-end pipeline inference latency have not yet been performed and are identified as priorities for immediate follow-up work before any real-time deployment claim can be fully supported.

Conclusions

The proposed hybrid surrogate–physics–AI optimization framework (H-SGP-BO–PINN–DRL) has been demonstrated to enhance both the energy efficiency and penetration rate in Tunnel Boring Machine (TBM) operations simultaneously. By integrating surrogate modeling, Bayesian optimization, physics-informed constraints, and deep reinforcement learning, the framework achieved accelerated convergence, reduced computational costs, and improved operational stability under variable geological conditions. The combination of data-driven intelligence and physics-based regularization provides a balanced mechanism between performance improvement and physical feasibility, ensuring that optimized solutions remain consistent with the underlying mechanics of the ground–machine interaction. Convergence analyses indicated that the hybrid model reached optimal solutions more rapidly and consistently than conventional metaheuristic algorithms such as GA, PSO, and SA. This improvement highlights the synergistic contribution of Bayesian-guided parameter adaptation and reinforcement learning-based control refinement. The multi-objective optimization results further confirmed that the proposed approach successfully minimized the Specific Energy Consumption (SEC) while maximizing the Penetration Rate (PR), achieving a more favorable SEC–PR trade-off than that of the traditional models.

From a methodological standpoint, the integration of physics-informed neural networks (PINN) and deep reinforcement learning (DRL) represents a significant advancement in intelligent tunneling optimization. The inclusion of mechanical equilibrium constraints within the learning architecture ensured that all predicted parameters complied with the principles of rock and soil mechanics, whereas the adaptive control layer continuously refined operational decisions based on environmental feedback. This hierarchical structure transformed the optimization framework from a static algorithmic process to a dynamic, self-adaptive learning system capable of cycle-wise adaptive decision support Taken together, these findings suggest that the H-SGP-BO–PINN–DRL framework not only provides a technically robust and computationally efficient solution but also establishes a theoretical foundation for the next generation of intelligent, physics-consistent TBM control systems.

In summary, this study presents a novel paradigm for TBM performance optimization that bridges the gap between physical modeling and artificial intelligence. The proposed hybrid approach offers a pathway toward autonomous, energy-efficient, and geotechnically reliable tunneling operations that can be used for the construction of tunnels. By unifying surrogate-based learning, physics-informed constraints, and adaptive reinforcement control, the framework contributes to both academic understanding and industrial application, paving the way for future integration into smart TBM systems capable of self-correcting optimization, pending the temporal-architecture and latency work identified in the Limitations and Future Work section.

Acknowledgement

This research was funded by the Ministry of Higher Education, Science, and Technology (Kemdiktisaintek) through the Beginner Lecturer Research (Penelitian Dosen Pemula, PDP) Scheme, Batch II, Fiscal Year 2025.

References

[1] X. Fu, M. Wu, R. L. K. Tiong, and L. Zhang, "Data-driven joint multi-objective prediction and optimization for advanced control during tunnel construction," *Expert Syst Appl*, vol. 238, p. 122118, 2023, doi: https://doi.org/10.1016/j.eswa.2023.122118.

[2] W. Liu, A. Li, and C.-Y. Liu, "Multi-objective optimization control for tunnel boring machine performance improvement under uncertainty," *Autom. Constr.*, 2022, doi: https://doi.org/10.1016/j.autcon.2022.104310.

[3] X. Wang *et al.*, "QPSO-ILF-ANN-based optimization of TBM control parameters considering tunneling energy efficiency," *Front. Struct. Civ. Eng.*, vol. 17, pp. 25–36, 2023, doi: https://doi.org/10.1007/s11709-022-0908-z.

[4] Z. Ma, G. Wu, P. Suganthan, A. Song, and Q. Luo, "Performance assessment and exhaustive listing of 500+ nature inspired metaheuristic algorithms," *Swarm Evol Comput*, vol. 77, p. 101248, 2022, doi: https://doi.org/10.48550/arxiv.2212.09479.

[5] K. Rajwar, K. Deep, and S. Das, "An exhaustive review of the metaheuristic algorithms for search and optimization: taxonomy, applications, and open challenges," *Artif. Intell. Rev.*, pp. 1–71, 2023, doi: https://doi.org/10.1007/s10462-023-10470-y.

[6] B. Toaza and D. Esztergár-Kiss, "A review of metaheuristic algorithms for solving TSP-based scheduling optimization problems," *Appl Soft Comput*, vol. 148, p. 110908, 2023, doi: https://doi.org/10.1016/j.asoc.2023.110908.

[7] O. Turgut, M. Turgut, and E. Kırtepe, "A systematic review of the emerging metaheuristic algorithms on solving complex optimization problems," *Neural Comput. Appl.*, vol. 35, pp. 14275–14378, 2023, doi: https://doi.org/10.1007/s00521-023-08481-5.

[8] C. Salam M and A. Khanifa, "An Interpretable Data-Driven Framework for Smart Tunnel Boring Machine Performance Analysis and Energy–Cost Optimization," *J. Tek. Ind. J. Keilmuan Dan Apl. Tek. Ind.*, vol. 28, no. 1, pp. 24–46, 2026, doi: https://doi.org/10.9744/jti.28.1.24-46.

[9] B. Abdollahzadeh *et al.*, "Puma optimizer (PO): a novel metaheuristic optimization algorithm and its application in machine learning," *Clust Comput*, vol. 27, pp. 5235–5283, 2024, doi: https://doi.org/10.1007/s10586-023-04221-5.

[10] A. Alorf, "A survey of recently developed metaheuristics and their comparative analysis," *Eng Appl Artif Intell*, vol. 117, p. 105622, 2023, doi: https://doi.org/10.1016/j.engappai.2022.105622.

[11] W. Yi, R. Qu, L. Jiao, and B. Niu, "Automated Design of Metaheuristics Using Reinforcement Learning Within a Novel General Search Framework," *IEEE Trans. Evol. Comput.*, vol. 27, pp. 1072–1084, 2023, doi: https://doi.org/10.1109/tevc.2022.3197298.

[12] V. Goyal and J. Grand-Clément, "Robust Markov Decision Processes: Beyond Rectangularity," *Math Oper Res*, vol. 48, pp. 203–226, 2022, doi: 10.1287/moor.2022.1259.

[13] P. Qu and L. Zhang, "Uncertainty-based multi-objective optimization in twin tunnel design considering fluid-solid coupling," *Reliab Eng Syst Saf*, vol. 253, p. 110575, 2024, doi: https://doi.org/10.1016/j.ress.2024.110575.

[14] Y. Wang, C. Ye, and Y. Wang, "Hierarchical multi-objective optimization of proton exchange membrane fuel cell with parameter uncertainty," *Swarm Evol Comput*, vol. 86, p. 101464, 2024, doi: https://doi.org/10.1016/j.swevo.2023.101464.

[15] N. Hassan and A. Saleem, "Neural Network-Based Adaptive Controller for Trajectory Tracking of Wheeled Mobile Robots," *IEEE Access*, vol. 10, pp. 13582–13597, 2022, doi: https://doi.org/10.1109/access.2022.3146970.

[16] X. Li, L. Wang, Y. An, Q. Huang, Y. Cui, and H. Hu, "Dynamic path planning of mobile robots using adaptive dynamic programming," *Expert Syst Appl*, vol. 235, p. 121112, 2023, doi: https://doi.org/10.1016/j.eswa.2023.121112.

[17] L. Zhang, Y. Li, L. Wang, J. Wang, and H. Luo, "Physics-data driven multi-objective optimization for parallel control of TBM attitude," *Adv Eng Inform.*, vol. 65, p. 103101, 2025, doi: https://doi.org/10.1016/j.aei.2024.103101.

[18] S. Hou, Y. Liu, J. Yu, R. Zhang, L. Cheng, and C. Gao, "Intelligent decision-making for TBM tunnelling control parameters using multi-objective optimization," *J. Rock Mech. Geotech. Eng.*, 2024, doi: https://doi.org/10.1016/j.jrmge.2024.09.001.

[19] F. Shan, X. He, D. J. Armaghani, and D. Sheng, "Effects of data smoothing and recurrent neural network (RNN) algorithms for real-time forecasting of tunnel boring machine (TBM) performance," *J. Rock Mech. Geotech. Eng.*, 2023, doi: https://doi.org/10.1016/j.jrmge.2023.06.015.

[20] K. Rajwar, K. Deep, and S. Das, "An exhaustive review of the metaheuristic algorithms for search and optimization: taxonomy, applications, and open challenges," *Artif. Intell. Rev.*, pp. 1–71, 2023, doi: https://doi.org/10.1007/s10462-023-10470-y.

[21] C. Salam M, M. Rinjani, O. Kural, M. Rinduwidara, and A. Khanifa, "Enhancing output in open-pit coal mining: The influence of front-loading geometry on machinery functionality," *Concurr. Eng.*, vol. 33, no. 1–4, pp. 145–170, Dec. 2025, doi: https://doi.org/10.1177/1063293X251361192.

[22] G. V. Priya and S. Ganguly, "Multi-swarm surrogate model assisted PSO algorithm to minimize distribution network energy losses," *Appl Soft Comput*, vol. 159, p. 111616, 2024, doi: https://doi.org/10.1016/j.asoc.2024.111616.
[23] A. Younis and Z. Dong, "Adaptive surrogate assisted multi-objective optimization approach for highly nonlinear and complex engineering design problems," *Appl Soft Comput*, vol. 150, p. 111065, 2023, doi: https://doi.org/10.1016/j.asoc.2023.111065.
[24] H. Kim, C. Park, and H. Kim, "Multi-task optimization with Bayesian neural network surrogates for parameter estimation of a simulation model," *Comput Stat Data Anal*, vol. 204, p. 108097, 2024, doi: https://doi.org/10.1016/j.csda.2024.108097.
[25] Q. Lin, J. Hu, and Q. Zhou, "Parallel multi-objective Bayesian optimization approaches based on multi-fidelity surrogate modeling," *Aerosp. Sci. Technol.*, 2023, doi: https://doi.org/10.1016/j.ast.2023.108725.
[26] R. R. Faria, B. Capron, A. Secchi, and M. B. de Souza, "A data-driven tracking control framework using physics-informed neural networks and deep reinforcement learning for dynamical systems," *Eng Appl Artif Intell*, vol. 127, p. 107256, 2024, doi: https://doi.org/10.1016/j.engappai.2023.107256.
[27] M. H. Saeed, H. Kazmi, and G. Deconinck, "Dyna-PINN: Physics-informed Deep Dyna-Q Reinforcement Learning for Intelligent Control of Building Heating System in Low-Diversity Training Data Regimes," *Energy Build.*, 2024, doi: https://doi.org/10.1016/j.enbuild.2024.114879.
[28] K. Elbaz, A. Zhou, and S. Shen, "Deep reinforcement learning approach to optimize the driving performance of shield tunnelling machines," *Tunn. Undergr. Space Technol.*, 2023, doi: https://doi.org/10.1016/j.tust.2023.105104.
[29] E. Soranzo, C. Guardiani, and W. Wu, "Reinforcement Learning for the Face Support Pressure of Tunnel Boring Machines," *Geosciences*, 2023, doi: https://doi.org/10.3390/geosciences13030082.
[30] E. Martinez, F. Stauch, B. G. de Soto, and R. Sacks, "Integration of building information modelling and digital twin in mechanized tunnelling construction," *Eng. Constr. Archit. Manag.*, 2025, doi: https://doi.org/10.1108/ecam-01-2025-0031.
[31] S. Mostafa, R. L. Sousa, and H. H. Einstein, "Toward the automation of mechanized tunneling 'exploring the use of big data analytics for ground forecast in TBM tunnels,'" *Tunn. Undergr. Space Technol.*, 2024, doi: https://doi.org/10.1016/j.tust.2024.105643.
[32] J. Huang, A. Ji, L. Zhang, X. Fu, and X. Song, "Data-driven optimization for enhanced excavation efficiency in tunnel construction: A case study," *Eng Appl Artif Intell*, vol. 142, p. 109868, 2025, doi: https://doi.org/10.1016/j.engappai.2024.109868.
[33] Y. Pan, Z. Wang, L. Sun, and J. Chen, "Dynamic prediction and multi-objective optimization on driving position of tunnel boring machine (TBM): an automated deep learning approach," *Acta Geotech.*, 2024, doi: https://doi.org/10.1007/s11440-024-02271-6.
[34] M. Ahmad, S. Keawsawasvong, M. R. Bin Ibrahim, M. Waseem, K. Reza Kashyzadeh, and M. M. Sabri Sabri, "Novel Approach to Predicting Soil Permeability Coefficient Using Gaussian Process Regression," *Sustainability*, vol. 14, no. 14, p. 8781, 2022, doi: https://doi.org/10.3390/su14148781.
[35] P. Aivaliotis-Apostolopoulos and D. Loukidis, "Swarming genetic algorithm: A nested fully coupled hybrid of genetic algorithm and particle swarm optimization," *PLoS ONE*, vol. 17, 2022, doi: https://doi.org/10.1371/journal.pone.0275094.
[36] Karishma and H. Kumar, "A novel hybrid model for task scheduling based on particle swarm optimization and genetic algorithms," *Math. Eng.*, 2024, doi: https://doi.org/10.3934/mine.2024023.
[37] W. Ouyang, G. Li, L. Chen, and S.-W. Liu, "Machine learning-based soil–structure interaction analysis of laterally loaded piles through physics-informed neural networks," *Acta Geotech.*, 2024, doi: https://doi.org/10.1007/s11440-023-02179-7.
[38] H. Zhou, H. Wu, B. B. Sheil, and Z. Wang, "A self-adaptive physics-informed neural networks method for large strain consolidation analysis," *Comput. Geotech.*, 2025, doi: https://doi.org/10.1016/j.compgeo.2025.107131.
[39] P. Lin, A. Ji, Y. Zhou, L. Zhang, and R. L. K. Tiong, "Automated position control of tunnel boring machine during excavation using deep reinforcement learning," *Appl Soft Comput*, vol. 167, p. 112234, 2024, doi: https://doi.org/10.1016/j.asoc.2024.112234.
[40] P. Lin, L. Zhang, R. L. K. Tiong, and X. Song, "Physics-guided deep reinforcement learning for improved operation of TBM considering kinetic inertia stability," *Adv Eng Inform.*, vol. 63, p. 102943, 2025, doi: https://doi.org/10.1016/j.aei.2024.102943.
[41] K. Fu, A. Ye, and L. Zhou, "Parameterized fragility-based uncertainty influence quantification and sensitivity analysis methodology: Concept, formulation, and application," *Soil Dyn. Earthq. Eng.*, 2025, doi: https://doi.org/10.1016/j.soildyn.2024.109070.
[42] V. Karyofylli *et al.*, "Sensitivity analysis and uncertainty quantification in predictive modeling of proton-exchange membrane electrolytic cells," *J. Power Sources*, 2024, doi: https://doi.org/10.1016/j.jpowsour.2024.234209.